is not pure spin–lattice in nature but has a considerable spin–spin (T_2) component due to rapid ^1H spin diffusion between the different phases.[23] In highly crystalline systems, the rotating-frame relaxation $T_{1\rho}$ was found to be completely dominated by spin–spin relaxation.[24] In such systems, the $T_{1\rho}$ of the crystalline phase is usually *shorter* than the amorphous region because of more efficient T_2 in the crystalline region. In these nylon 6 samples, however, the $T_{1\rho N}$ values mimic the T_{1N} data. Spin diffusion, although highly evident in the nearly identical T_{1H} values for both the crystalline and amorphous phases, does not dominate $T_{1\rho N}$. Nevertheless, the *two* amorphous components seen in the T_{1N} relaxation experiment are not evident from $T_{1\rho N}$ measurements. Similar to the T_{1N} data, the increase in $T_{1\rho N}$ of the *crystalline* component may be related to changing crystallite size.

Conclusions

The ^{15}N-labeled nylon 6 sample was prepared in good yield by anionic polymerization of the ^{15}N-labeled ϵ-caprolactam monomer. Enrichment of approximately 20% ^{15}N has allowed direct T_{1N} and $T_{1\rho N}$ relaxation measurements as well as T_{1H} determination by indirect observation of ^{15}N cross polarization.

As expected, the rigid crystalline region has a much longer T_{1N} relaxation than the more mobile amorphous region. The T_{1N} of the crystalline fraction was 111–416 s. Two components were observed in the relaxation of the amorphous peak: a fast component with T_1 of 1–3 s and a longer component with T_1 of 19–29 s. The two noncrystalline components are thought to belong to amorphous and noncrystalline interphase regions, respectively.

Less dramatic behavior is seen in $T_{1\rho N}$ relaxation times. Only a single amorphous component could be observed. This anomaly is attributed to considerable ^1H spin–spin relaxation within the sample resulting in similar $T_{1\rho N}$ values. This conclusion is further supported by ^1H T_1 relaxation experiments, which show that rapid ^1H spin diffusion is occurring between the phases. Addition of plasticizers, which concentrate in the amorphous region, apparently decreases the observed $T_{1\rho N}$ of both the crystalline and amorphous regions. However, the effect on the crystalline $T_{1\rho N}$ may be better attributed to differences in crystallite size than to increased motion.

The first chemical shift anisotropy patterns of a polyamide have been obtained on nylon 6. The CSA powder patterns show the growth of an amorphous signal at elevated temperatures with a chemical shift near the isotropic value obtained with MAS. The addition of plasticizer (caprolactam) causes this signal to grow in at lower temperatures, confirming that plasticization is increasing molecular mobility in the amorphous region. The σ_{33} component becomes less prominent with increasing temperature and finally disappears above 115 °C. The phenomenon has not been previously reported but is postulated to be the result of anisotropic motion associated with the tensor component σ_{33}, which lies along the NH bond of the amide group.

Acknowledgment. We gratefully acknowledge a Department of Defense instrumentation grant with which we purchased our Bruker MSL-200 spectrometer. This research was supported in part by a grant from the Office of Naval Research. We also thank Dr. William L. Jarrett for helpful discussions concerning the NMR pulse experiments reported here.

Registry No. Nylon 6, 25038-54-4; ϵ-caprolactam, 105-60-2.

(22) Menger, E. M.; Veeman, W. S.; de Boer, E. *Macromolecules* **1982**, *15*, 1406.
(23) Veeman, W. S.; Menger, E. M. *Bull. Magn. Reson.* **1980**, *2*, 77.
(24) VanderHart, D. L.; Garroway, A. N. *J. Chem. Phys.* **1979**, *71*, 2773.

A Quantitative Clarification of Vibrationally Coupled Dioxygen in the Resonance Raman Spectra of Cobalt-Substituted Heme Proteins and Model Compounds

Leonard M. Proniewicz[1] and James R. Kincaid*

Contribution from the Chemistry Department, Marquette University, Milwaukee, Wisconsin 53233. *Received April 24, 1989*

Abstract: The resonance Raman (RR) spectra of dioxygen adducts of cobalt porphyrin complexes with various trans-axial bases and cobalt-substituted heme proteins exhibit complicated spectral patterns characterized by the appearance of weak secondary features and unexpected frequencies and intensities of the ν(O–O) of the various dioxygen isotopomers. These patterns are shown to derive from vibrational resonance coupling of ν(O–O) with internal modes of the trans-axial ligand. The observed frequency perturbations and intensities agree, within experimental error, with those calculated by using the conventional Fermi resonance coupling scheme. Further, it is shown that a careful quantitative treatment of spectral data for the proteins provides accurate estimates of the frequencies of particular modes associated with the coordinated histidylimidazole fragment.

Vibrational spectroscopy has long served as a powerful probe of the structure and bonding of dioxygen adducts of metal complexes.[2,3] It is therefore not surprising that much effort has been devoted to its utilization for the study of the O_2 adducts of nature's oxygen transport proteins, hemoglobin (Hb) and myoglobin (Mb), inasmuch as it potentially provides a relatively convenient and sensitive method to directly monitor even subtle changes in structure and bonding of the metal–oxygen linkage. While some important new information has been gained from both infrared[4] and resonance Raman spectroscopies,[5,6] several problems have prevented these techniques from providing information at a level of sophistication which is commensurate with their inherent promise.

The problems encountered for IR studies essentially arise from the experimental difficulties associated with extracting the ν(O–O) and ν(M–O) absorptions from those due to the protein matrix.[4]

(1) Permanent address: Regional Laboratory of Physicochemical Analyses and Structural Research, Jagiellonian Univeristy, Cracrow, Poland.
(2) Nakamoto, K. *Infrared and Raman Spectra of Inorganic and Coordination Compounds*; Wiley-Interscience: New York, 1986; p 414.
(3) Nakamoto, K. *Coord. Chem. Rev.*, in press.
(4) Caughey, W. S. In *Methods for Determining Metal Ion Environments in Proteins: Structure and Function of Metalloproteins*; Darnall, D. W.; Wilkins, R. G., Eds.; Elsevier: North Holland, New York, 1980; p 95.
(5) Spiro, T. G. In *Iron Porphyrins*; Lever, A. B. P., Gray, H. B., Eds.; Addison-Wesley Publishing Co.: Reading, MA, 1983; Part II, p 89.
(6) Yu, N.-T., Kerr, E. A. In *Biological Applications of Raman Spectroscopy*; Spiro, T. G., Ed.; Wiley-Interscience: New York, 1987; Vol. 3, p 39.

0002-7863/90/1512-675$02.50/0

Thus, in contrast to IR studies of the corresponding carbon monoxide adducts, where the ν(C–O) is easily observed as an isolated intense band in an uncluttered region of the spectrum, the ν(O–O) of the dioxygen adducts are weak and occur in a spectral region which contains intense background absorption from the protein backbone and amino acid side chains. The severe experimental problems and the resulting difficulties of spectral interpretation are nicely described in a thorough study recently reported by Caughey and co-workers.[7]

In principle, RR spectroscopy offers a more attractive approach in that the vibrational modes of the chromophore (in this case, the heme–O_2 adduct) may, in favorable circumstances, be selectively enhanced by several orders of magnitude over those of the protein matrix. While Nakamoto and co-workers have recently shown that ν(O–O) of a model heme–O_2 adduct is enhanced with 406.7-nm excitation,[8] no such enhancement of the native protein systems is observed with this excitation wavelength or with any other yet utilized.[5,6] Fortunately, Yu and co-workers[9] discovered that ν(O–O) and ν(Co–O) are efficiently enhanced (at 406.7-nm excitation) in the case of the cobalt-substituted analogues and have applied the method to the study of several proteins.[6] However, the observed spectra are severely complicated by the appearance of multiple oxygen-isotope sensitive bands and unexpected intensity patterns.[6,9] These spectra were reasonably interpreted in terms of two coexistent solution structures, in agreement with a reported crystal structure of oxy-myoglobin.[10] Recently, we reported extended studies of these adducts and offered an alternative interpretation which invoked vibrational coupling of the bound O_2 with internal modes of the proximal (and possibly the distal) histidylimidazole and which does not require the existence of two structures.[11] The plausibility of this interpretation was supported by concurrent and previous model compound studies which documented such vibrational interactions.[12-14]

While the existence of vibrational coupling in each of these earlier works was clearly demonstrated by isotopic substitution, the actual number of different coupling interactions was rather small, and no effort was made to relate the observed frequency shifts and relative intensities of the coupled pairs to theoretical predictions, although it was pointed out that they generally approximated the behavior expected for coupled oscillators.[14] However, we have recently completed an extensive study of O_2 adducts of cobalt–porphyrin complexes with imidazole and several of its selectively deuteriated analogues.[15] In addition, we are currently studying the effects of base orientation and axial ligand structure on coupling strength.[16] Provided with this larger data set, we now apply existing theory to the various O_2 adducts thus far studied and illustrate that (within experimental error) the calculated frequencies and relative intensities of all of the coupled modes agree with those observed.[11-16]

Results and Discussion

A. Theoretical Framework. As is fully described in the standard reference work on vibrational transitions and spectroscopy,[17] anharmonicity may lead to interactions of normal modes giving rise to frequency perturbations of the coupled modes from their inherent frequencies and mixing of the vibrational eigenfunctions. Such interactions are adequately treated by first-order perturbation theory which leads to the following expression for the new frequencies (using a modification of Herzberg's notation).

$$\nu = \nu_{ni} \pm \tfrac{1}{2}(4W_{ni}^2 + \delta^2)^{1/2} \quad (1)$$

In this expression

$$\nu_{ni} = \tfrac{1}{2}(\nu_n^\circ + \nu_i^\circ)$$

i.e., the average value of the unperturbed frequencies of the coupled modes

$$\delta = (\nu_n^\circ - \nu_i^\circ)$$

i.e., the separation of the unperturbed levels. Finally, W_{ni} is the matrix element of the perturbation function W in the equation

$$W_{ni} = \int \Psi_n^\circ W \Psi_i^{\circ *} d\tau \quad (2)$$

where Ψ_n° and Ψ_i° are the nonperturbed eigenfunctions of the two levels which interact, and W is determined by the anharmonic terms in the potential energy. Thus, it is seen that two levels of the same symmetry (since W is totally symmetric, Ψ_n° and ψ_i° must belong to the same symmetry class) will repel each other, each shifting by $^1/_2(4W_{ni}^2 + \delta^2)^{1/2}$ from the average value, and that the shifts from the unperturbed values increase as the separation decreases (see Figure 70 of ref 17).

In eq 1 W_{ni} is an energy term which can be derived from known values for the perturbed and unperturbed frequencies (vide infra). Such experimentally determined values of W_{ni} include a factor which depends on the effective mass of the coupled modes. Thus, in the cases of interest here, the derived W_{ni} will depend on the reduced mass of the ν(O–O) and that of the internal ligand mode. Clearly, the relative W_{ni} values for $^{16}O_2$ coupling to different ligand modes cannot be easily estimated since there is ambiguity in defining effective reduced masses for internal ligand modes. On the other hand, it is useful to consider the expected relative values of W_{ni} for coupling of different dioxygen isotopomers with the same internal ligand mode. Thus, while the inherent coupling strength is independent of the oxygen isotopomer employed, the experimentally determined W_{ni} values are expected to vary in the following manner:[18]

$$W_{ni}(^{16}O_2):W_{ni}(^{16}O^{18}O):W_{ni}(^{18}O_2) \approx 1.00:0.985:0.970$$

Utilization of these expected relative values is useful in calculating W_{ni} and the unperturbed frequencies of ν(O–O) and internal ligand modes from the observed (i.e., perturbed) frequencies and intensities (vide infra).

The vibrational interaction also leads to mixing of the eigenfunctions according to the following equations derived from perturbation theory:[17]

$$\Psi_n = a\Psi_n^\circ - b\Psi_i^\circ \quad (3a)$$

$$\Psi_i = b\Psi_n^\circ + a\Psi_i^\circ \quad (3b)$$

where

$$a = \left(\frac{(4W_{ni}^2 + \delta^2)^{1/2} + \delta}{2(4W_{ni}^2 + \delta^2)^{1/2}} \right)^{1/2}$$

and

$$b = \left(\frac{(4W_{ni}^2 + \delta^2)^{1/2} - \delta}{2(4W_{ni}^2 + \delta^2)^{1/2}} \right)^{1/2}$$

The above equations were derived for the interaction of a fundamental with an overtone or combination mode of the same symmetry and were first applied by Fermi to explain the appearance of two bands near 1300 cm^{-1} ($\nu(C–O)_{sym}$) in the spectrum of CO_2.[19] However, Lax[20] has shown that similar equations result for the coupling of two fundamentals in solids, and his approach

(7) Potter, W. T.; Tucker, M. P.; Houtchens, R. A.; Caughey, W. S. *Biochemistry* **1987**, *26*, 4699.
(8) Wagner, W. D.; Paeng, I. R.; Nakamoto, K. *J. Am. Chem. Soc.* **1988**, *110*, 5565.
(9) Tsubaki, M.; Yu, N.-T. *Proc. Natl. Acad. Sci. U.S.A.* **1981**, *78*, 3581.
(10) Shaanan, B. *J. Mol. Biol.* **1983**, *171*, 31.
(11) Bruha, A.; Kincaid, J. R. *J. Am. Chem. Soc.* **1988**, *110*, 6006.
(12) Bajdor, K.; Kincaid, J. R.; Nakamoto, K. *J. Am. Chem. Soc.* **1984**, *106*, 7741.
(13) Kincaid, J. R.; Proniewicz, L. M.; Bajdor, K.; Bruha, A.; Nakamoto, K. *J. Am. Chem. Soc.* **1985**, *107*, 6775.
(14) Proniewicz, L. M.; Nakamoto, K.; Kincaid, J. R. *J. Am. Chem. Soc.* **1988**, *110*, 4541.
(15) Proniewicz, L. M.; Bruha, A.; Nakamoto, K.; Kyuno, E.; Kincaid, J. R. *J. Am. Chem. Soc.*, in press.
(16) Proniewicz, L. M.; Bruha, A.; Uemori, Y.; Nakamoto, K.; Kyuno, E.; Kincaid, J. R. To be submitted for publication.
(17) Herzberg, G. *Molecular Spectra and Structure*; Van Nostrand: New York, 1945; Vol. 2, p 215.
(18) The relative values actually depend both on the reduced mass and inherent frequencies of the vibrational modes and are derived from the rigorous theoretical treatment as given, for example, in ref 25.
(19) Fermi, E. *Z. Phys.* **1931**, *71*, 250.
(20) Lax, M. *J. Phys. Chem. Solids* **1964**, *25*, 487.

has been applied to the analysis of Fermi resonances in fluid solution by many workers.[21-23]

Recently, Monecke[24] has discussed and extended these treatments and has pointed out that, for frequencies and anharmonicities normally encountered in molecules, the new expressions yield calculated results which are insignificantly different from those calculated by using eq 1. This justifies the application of eq 1 to the complete set of data obtained from our previous[11-14] and current[15,16] studies of the O_2 adducts.

In addition, during the course of this work, Veas and McHale[25] have developed a general and rigorously correct theoretical framework for treating resonance vibrational interactions of solute modes with those of an unrestricted number (N) of associated solvent molecules. While McHale's development represents an important contribution to the general problem of solute–solvent vibrational interactions (with no restrictions on N), for the special case where $N = 1$, the equations are essentially identical with the conventional Fermi resonance equations (i.e., eq 1 and 3). In fact, Veas and McHale successfully applied their equation to the coupling of ν(O–O) with the 3,5-dichloropyridine (DCP) fragment of Co(TPP-d_8)(DCP)(O_2), the experimental data having been previously reported.[14]

For our purposes we have employed the more familiar equations and terminology presented in Herzberg,[17] recognizing the fact that Monecke's arguments[24] and McHale's general theoretical treatment[25] provide the essential validation for use of these. Special considerations regarding the specific compounds of interest are discussed below.

B. Application to O_2 Adducts of Cobalt–Porphyrin Complexes. Difficulty arises in applying eq 1–3 to the O_2 adducts of interest in that the inherent frequencies of the internal ligand modes are not directly available; i.e., the mode gains intensity only as a consequence of coupling with ν(O–O) and only the *perturbed* ligand mode is observed. In general, one cannot employ the frequency observed for the free ligand since coordination frequently shifts ligand modes by 10 cm^{-1} or more.[15] Thus, as will be made evident in the following sections, successful application of the theory to interactions of this type requires a more complete data set for a given adduct. That is, either the interaction must be removed (e.g, by selective deuteriation of the ligand) to reveal the inherent ν(O–O), or (at least two) oxygen isotopomers, each of which interacts with the same internal ligand mode, must be employed.

The observed relative intensities of the perturbed ν(O–O) and internal ligand mode can also be employed to help determine the coupling strength (W_{ni}) and inherent frequencies. Thus, in the case of these O_2 adducts, a resonance enhanced ν(O–O) mode interacts with a nonresonance enhanced internal ligand mode. Enhancement of the ligand mode is a consequence of mixing of the eigenfunctions. Accordingly, the intensity of the "mainly ligand mode" is expected to increase proportionally with b^2 (eq 3b). Similarly, the intensity of the "mainly ν(O–O) feature" is decreased relative to its unperturbed value, the fractional intensity being given by a^2 (eq 3a). That is, the total scattering intensity is not affected by the interaction but is merely distributed between the coupled modes. For example, in the case of exact resonance ($\delta = 0$), $a = b = \sqrt{1/2}$, and it is seen that the perturbed levels are equal mixtures of $\Psi_n°$ and $\Psi_i°$. In this particular case, wherein the inherent intensities of the ligand mode approaches 0, the result is that two bands of *equal* intensity are observed. As is generally true for such coupling interaction, the bands are shifted by equal magnitudes (in opposite directions) from their inherent (in this case, common) frequencies.

It is worth pointing out that in special situations (as in the case of these O_2 adducts) where an "inactive" mode gains intensity by virtue of coupling with an active mode, the observed relative intensities together with the observed (i.e., perturbed) frequencies provide sufficient information to derive inherent frequencies and W_{ni} values. However, in practice, the small errors present in the experimental data lead to large uncertainties in the derived W_{ni} values and calculated inherent frequencies (i.e., more than 2 cm^{-1}). As will be seen in the following sections, utilization of multiple dioxygen isotopomers, taken together with the knowledge of relative W_{ni} values for the various isotopomers, provides additional restrictions on the combinations of inherent frequencies and W_{ni} values which will satisfy all of the above conditions (i.e., correct intensities and W_{ni} values of appropriate relative magnitudes).

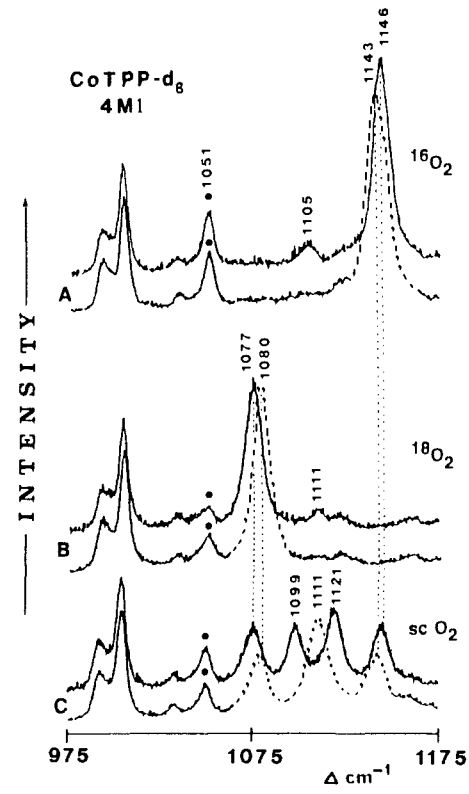

Figure 1. Resonance Raman spectra of dioxygen adducts of CoTPP-d_8 in the presence of 4-methylimidazole, 4MI (solid line), or its deuteriated analogue, 4MI-d_2 (broken line) in $C^2H_2Cl_2$ at ~−90 °C: (A) $^{16}O_2$, (B) $^{18}O_2$, and (C) $^{16}O_2$:$^{16}O^{18}O$:$^{18}O_2$ (1:2:1 by volume). Excitation at 406.7 nm. The 1051-cm^{-1} line (•) is due to $C^2H_2Cl_2$.

In the majority of the previous works[11-14] the opportunities for coupling in an individual complex were rather few, and systematic application of the theory was not presented, although approximate agreement was noted.[14] The total number of observed coupling interactions of this type (i.e., using various trans-axial bases) has now grown to the point which justifies a detailed comparison with theoretical predictions. The results for these systems are presented below.

1. Dioxygen Adducts of Co(TPP-d_8)(4-methylimidazole). One of the most striking illustrations of the spectral consequences associated with vibrationally coupled dioxygen was obtained during the study of O_2 adducts which contained a trans-axial 4-methylimidazole (4MI).[11] The spectra are reproduced here (Figure 1) in order to clearly illustrate the application of the equations provided in section A.

In Figure 1 the spectra illustrated with dotted lines correspond to those obtained for the complex with a deuteriated 4MI (i.e., 4MI-d_2) which possesses no internal modes of A_1 symmetry in the region between 1050 and 1150 cm^{-1}; i.e., there is no opportunity for vibrational coupling of ν(O–O) with the trans-axial base modes. Therefore, assignment of ν(^{16}O–^{16}O) to the strong band at 1143 cm^{-1} (trace A) and ν(^{18}O–^{18}O) to the 1080-cm^{-1} feature (trace B) are straightforward. Similarly, the spectrum of the adducts with "scrambled" O_2 (i.e., $^{16}O_2$:$^{16}O^{18}O$:$^{18}O_2$, 1:2:1 by volume) exhibits a ν(^{16}O–^{18}O) at 1111 cm^{-1} in addition to the

(21) Scott, J. F. In *Light Scattering in Solids*; Balkanski, M., Ed.; Flamarion: Paris, 1972; p 387.
(22) Wang, C. H.; McHale, J. L. *J. Chem. Phys.* **1980**, *72*, 4039.
(23) Irmer, G.; Toporov, V. V.; Bairamov, B. H.; Monecke, J. *Phys. Status Solidi B* **1983**, *119*, 595.
(24) Monecke, J. *J. Raman Spectrosc.* **1987**, *18*, 477.
(25) Veas, C.; mcHale, J. L. Submitted for publication.

1143- and 1080-cm^{-1} bands. The observed intensities are 1:2:1, as expected.

As can be seen in Figure 1 (solid lines), the spectra of the adducts with natural abundance 4MI are indicative of vibrationally coupled dioxygen. The $\nu(^{16}O-^{16}O)$ is shifted *up* by 3 cm^{-1} to 1146 cm^{-1} and a weak secondary feature is observed at 1105 cm^{-1}. In the case of the $^{18}O_2$ adduct (trace B), the $\nu(^{18}O-^{18}O)$ is shifted *down* by 3 cm^{-1} to 1077 cm^{-1}, and the weak secondary feature is now observed at 1111 cm^{-1} (i.e., 6 cm^{-1} higher than in trace A). Clearly, an internal imidazole mode near 1108 cm^{-1} is capable of interacting with $\nu(^{16}O-^{16}O)$ and $\nu(^{18}O-^{18}O)$ to yield such behavior. Thus, very strong coupling of the 1108-cm^{-1} mode with $\nu(^{16}O-^{18}O)$ (inherent frequency of 1111 cm^{-1}) is expected. This coupling is dramatically demonstrated (trace C, solid line) by the appearance of two strong bands of nearly equal intensity shifted by $\sim\pm10$ cm^{-1} from their inherent frequencies (i.e., 1121 - 1111 cm^{-1} $\approx$ 1108 - 1099 cm^{-1} $\sim$ 10 cm^{-1}).

The equations given in section A are applied to these data in the following manner. The observed and estimated inherent frequencies of both the ν(O–O) and ligand modes (for two or more dioxygen isotopomers if available) are used to calculate W_{ni} values and relative intensities with use of a BASIC program based on eq 1 and 3. The calculated intensities are then compared with those observed (integrated) intensities, and the relative W_{ni} values are also available for comparison. Slight adjustments of the input data are made until calculated intensities match those observed and W_{ni} values are of appropriate relative magnitude. During this fitting procedure, the perturbed frequency values which are used as input are maintained within experimental error of those actually observed. The value of the unperturbed ligand frequency (an unknown quantity) is also varied, but, of course, the same value is used for the different O_2 isotopomer cases. In addition, the inherent ν(O–O) values for the different dioxygen isotopomers are constrained by the relationship based on reduced masses (i.e., $\Delta\nu[^{16}O_2 - (^{16}O^{18}O)] = \Delta\nu[(^{16}O^{18}O)] - {}^{18}O_2] = 33$ cm^{-1}.

In summary, the iterative procedure described above is used to determine the values of inherent (unperturbed) frequencies and coupling parameters (W_{ni}) which reproduce, within experimental error, the observed (i.e., perturbed) frequencies and intensities. Agreement between the observed and calculated frequencies and intensities is taken as a demonstration of behavior which is consistent with the model, provided that the relative values of W_{ni} for the various dioxygen isotopomers are approximately correct (i.e., $W_{ni}(^{16}O_2):W_{ni}(^{16}O^{18}O):W_{ni}(^{18}O_2) \approx 1.00:0.985:0.970$).

The results of the application of this procedure to the O_2 adducts of Co(TPP-d_8) (4MI) are summmarized in Table I along with those obtained for other systems studied thus far. In order to avoid confusion, we wish to emphasize that certain entries in Table I needed to be adjusted for secondary solvent effects.[11] For example, the unperturbed $\nu(^{18}O-^{18}O)$ for the $^{18}O_2$ adduct of Co(TPP-d_8)(4MI-d_2) is given as 1078 cm^{-1} even though the observed inherent frequency (Figure 1, trace B, dotted line) is apparently 1080 cm^{-1}. As was previously noted,[11] there is an interaction of the 1051-cm^{-1} mode of $C^2H_2Cl_2$ with $\nu(^{18}O-^{18}O)$ which induces a shift up to 1080 cm^{-1}. The spectra obtained in $C^1H_2Cl_2$ exhibit strong $\nu(^{18}O-^{18}O)$ frequencies of this complex at 1078 cm^{-1} (4MI-d_2) and 1075 cm^{-1} (4MI), respectively.

2. Dioxygen Adducts of Cobalt "Jellyfish Porphyrin" ($CoAz_{piv}\alpha\alpha$) Complexes with Imidazole and Its Deuteriated Analogues. An example of the interaction of ν(O–O) with multiple internal modes of the axial ligand is encountered in the study of O_2 adducts of $CoAz_{piv}\alpha\alpha$ complexes of 2,4,5-trideuterioimidazole (Im-d_3).[15] In fact, both the $\nu(^{16}O-^{16}O)$ and the $\nu(^{16}O-^{18}O)$ interact with the same two internal ligand modes. The spectra of both dioxygen isotopomers are shown in Figure 2. On the basis of the Raman spectrum of (free) Im-d_3 (Figure 2A), the coordinated Im-d_3 is expected to possess two internal ligand modes of A_1 symmetry in this region, one near 1115 cm^{-1} and one near 1130 cm^{-1}.[15] The inherent (i.e., unperturbed) $\nu(^{16}O-^{16}O)$ and $\nu(^{16}O-^{18}O)$ are known to occur at 1144 and 1111 cm^{-1}, respectively (note: $\Delta\nu(^{16}O_2/^{16}O^{18}O) = 33$ cm^{-1}, as expected).[15] Thus, both internal ligand modes are fortuitously positioned to interact with both

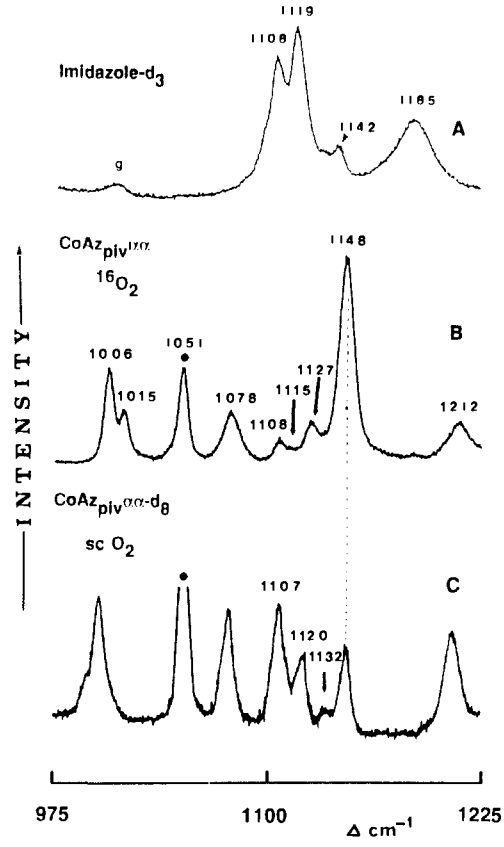

Figure 2. Resonance Raman spectra of dioxygen adducts of $CoAz_{piv}\alpha\alpha$ complex with 2,4,5-trideuterioimidazole (Im-d_3) in $C^2H_2Cl_2$ at $\sim$-90 °C (406.7-nm excitation: (B) $^{16}O_2$ and (C) $^{16}O_2$:$^{16}O-^{18}O$:$^{18}O_2$ ($\sim$1:2:1 by volume). Trace A: Raman spectrum of Im-d_3 in C^2HCl_3 at room temperature with excitation at 514.5 nm.

dioxygen isotopomer stretches. It is therefore expected that the $\nu(^{16}O-^{16}O)$ would couple with these inducing shifts to lower frequencies; the magnitude of each shift depending on the δ value for each. Conversely, interaction with $\nu(^{16}O-^{18}O)$ should lead to a slight increase in the frequency of each of these ligand modes.

As can be seen in Figure 2B, the $\nu(^{16}O-^{16}O)$ is observed at 1148 cm^{-1} (4 cm^{-1} higher than the inherent (1144 cm^{-1}) frequency), and two weak secondary features are observed at 1127 and 1115 cm^{-1}. In Figure 2C the $\nu(^{16}O-^{18}O)$ is observed at 1107 cm^{-1} (4 cm^{-1} lower than the 1111 cm^{-1} inherent value), and a rather intense secondary feature is observed at 1120 cm^{-1}. The other expected secondary feature is observed near 1132 cm^{-1}. Again, in order to avoid confusion, we point out that this is the spectrum of the scrambled oxygen mixture, so that the 1148-cm^{-1} as well as the weak 1127- and 1115-cm^{-1} features associated with the $^{16}O_2$ adduct also contribute to the spectrum given in Figure 2.C. While the region between 1110 and 1140 cm^{-1} is especially cluttered, the 2-fold proportion of $^{16}O^{18}O$:$^{16}O_2$ facilitates identification of the features (1107, 1120, and 1132 cm^{-1}) associated with the $^{16}O^{18}O$ isotopomer.

Inspection of the data given in Table I for these adducts clearly demonstrates that these complicated spectral patterns are precisely those predicted by using the program based on eq 1 and 3. Thus, employing inherent ligand frequencies of 1117 and 1131 cm^{-1} and inherent dioxygen frequencies of 1144 and 1111 cm^{-1}, the frequencies (with the accuracy $\pm$1cm^{-1}) and approximate intensities of all six perturbed modes are reproduced. In addition, the W_{ni} value for the $^{16}O^{18}O$ isotopomer case is $\sim$0.98 W_{ni} for the $^{16}O_2$ analogue, as required.

3. Other Model Compounds. In Table I we have also included the observed and calculated coupling patterns for O_2 adducts of Co(TPP-d_8)(pyridine) and Co(TPP-d_8)(3,5-dichloropyridine), the experimental data having been previously reported.[12,14] It is evident that the observed spectral patterns for these adducts are also consistent with expected behavior.

Table I. Summary of Observed and Calculated Frequencies and Intensities

					observed		calculated		
no.	base	O_2 isotopomer	ν_o^i	ν_L^i	$\nu_o(I_o)$	$\nu_L(I_L)$	$\nu_o(I_o)$	$\nu_L(I_L)$	W_{ni}
					Co(TPP-d_8)				
1.	4MI	$^{16}O_2$	1143	1108	1146 (0.91)	1105 (0.09)	1146 (0.93)	1105 (0.07)	10.68
2.	4MI	$^{16}O^{18}O$	1110	1108	1121 (0.57)	1099 (0.43)	1119.5 (0.55)	1098.5 (0.45)	10.45
3.	4MI	$^{18}O_2$	1077	1108	1074 (0.92)	1111 (0.08)	1074 (0.92))	1111 (0.08)	10.10
4.	DCP	$^{16}O_2$	1156	1115	1160 (0.91)	1112 (0.09)	1159.4 (0.93)	1111.5 (0.07)	12.48
5.	DCP	$^{16}O^{18}O$	1123	1115	1132 (0.63)	1108 (0.37)	1131.9 (0.65)	1106 (0.35)	12.36
6.	DCP	$^{18}O_2$	1090	1115	1086 (0.84)	1121 (0.16)	1084.9 (0.86)	1120 (0.14)	12.25
7.	P_y	$^{18}O_2$	1081	1069	1084 (0.88)	1067 (0.12)	1084 (0.83)	1066 (0.17)	6.71
8.	P_y	$^{16}O^{18}O$	1114	1069	1115 (0.93)	1067 (0.07)	1115 (0.98)	1068 (0.02)	6.78
					Co($Az_{piv}\alpha\alpha$)				
9.	Im	$^{16}O_2$	1144	1153	1138 (0.75)	1158 (0.25)	1139 (0.74)	1158 (0.26)	8.37
10.	Im[i]	$^{18}O_2$	1078	1072	1082 (0.68)	1068 (0.32)	1082 (0.71)	1068 (0.29)	6.32
11.	Im[a]	$^{16}O_2$	1144	1131	1148 (0.84)	1127 (0.16)	1148 (0.81)	1127 (0.19)	8.25
12.	Im[a,i]	$^{18}O_2$	1078	1067	1082 (0.71)	1063 (0.29)	1082.5 (0.76)	1063.5 (0.24)	8.08
13.	Im-d_1	$^{16}O_2$	1144	1150	1137 (0.70)	1156 (0.30)	1138 (0.67)	1156 (0.33)	8.49
14.	Im-d_1[i]	$^{18}O_2$	1078	1087	1076 (0.85)	1089 (0.15)	1076 (0.85)	1089 (0.15)	4.69
15.	Im-d_2[i]	$^{16}O^{18}O$	1111	1114	1106 (0.62)	1119 (0.38)	1106 (0.62)	1119 (0.38)	6.32
16.	Im-d_3	$^{16}O_2$	1144	1117	1148 (0.84)	1115 (0.02)	1146 (0.94)	1115 (0.06)	7.62
17.	Im-d_3	$^{16}O^{18}O$	1111	1117	1107 (0.58)	1120 (0.34)	1106 (0.69)	1122 (0.31)	7.42
18.	Im-d_3	$^{16}O_2$	1144	1131	1148 (0.84)	1127 (0.14)	1147 (0.84)	1128 (0.16)	6.93
19.	Im-d_3[i]	$^{16}O^{18}O$	1111	1131	1107 (0.58)	1132 (0.08)	1109 (0.92)	1133 (0.08)	6.63
					CoHb (H_2O or ^2H_2O)[b]				
20.	His	$^{16}O_2$	1139	1148	1136 (0.86)[c]	1150 (0.14)[c]	1136 (0.80)	1151 (0.20)	6.00
21.	His	$^{16}O_2$	1139	1109	*d*	1107 (weak)	1141 (0.94)	1107 (0.06)	9.52[f]
22.	His	$^{16}O^{18}O$	1106	1109	1098 (?)	*e*	1098 (0.58)	1117 (0.42)[d]	9.38
23.	His	$^{16}O^{18}O$	1106	1085	*d*	1080 (weak)	1113 (0.80)	1078 (0.20)[d]	13.96[f]
24.	His	$^{18}O_2$	1073	1085	1063 (0.78)	1093 (0.22)	1064 (0.70)	1094 (0.30)	13.75
25.	His	$^{16}O_2$	1139	1109	1140 (?)	1108 (weak)	1141 (0.94)	1107 (0.06)	9.52[g]
26.	His	$^{16}O^{18}O$	1106	1109	1098 (?)	*e*	1098 (0.58)	1117 (0.42)	9.38[g]
27.	His	$^{16}O^{18}O$	1106	1089	*d*	*d*	1109 (0.87)	1086 (0.13)	7.67[f]
28.	His	$^{18}O_2$	1073	1089	1070 (0.79)	1093 (0.21)	1070 (0.86)	1092 (0.14)	7.55

[a] Imidazole free from hydrogen bonding. [b] Entries 20–24 obtained from H_2O solution, entries 25–28 obtained from ^2H_2O solution. [c] Intensity calculated from data in ref 9. [d] These features derived from a second interaction. Observed features are determined by the primary interaction. [e] Band obscured by overlap with porphyrin macrocycle mode. [f] Calculated frequencies and intensities were obtained by using W_{ni} values derived from the W_{ni} value of the corresponding dioxygen isotopomer (e.g., 9.52 obtained as 9.38 × 1.0/0.985). [g] The frequencies and intensities are calculated by using the same W_{ni} as was used for H_2O (i.e., 9.52). [h] In all cases integrated intensities were used as observed intensities. [i] Co($Az_{piv}\alpha\alpha$-d_8) used for this case.

C. Application to O_2 Adducts of Cobalt-Substituted Hemoglobin and Myoglobin. The procedure outlined above can be applied to the spectra of O_2 adducts of the protein systems in an attempt to provide a quantitative treatment of our previously reported qualitative arguments.[11] However, it must be pointed out that such attempts are somewhat hindered by the inability to eliminate or control the vibrational coupling as was accomplished in the study of model compounds.

Thus, in the model systems, fully deuteriated ligands can be used to reveal the inherent ν(O–O), and deuteriated porphyrins (e.g., Co(TPP-d_8)) can be employed to remove overlapping macrocycle modes. Such manipulations are not easily accomplished in the case of the protein systems. In addition, the inherent frequencies of the internal modes of the coordinated histidyl-imidazole fragment are not known since conditions for direct resonance enhancement of these have not been identified. While systematic application of the procedure to the proteins is thus hampered by the considerations outlined above, it is satisfying to point out that the observed frequencies and intensities can be closely approximated with eq 1–3 by making several assumptions which are *well-supported* by existing data.

The spectra of six proteins were presented and discussed qualitatively in our previous work.[11,26] For our present purpose, we focus on the spectra of the O_2 adducts of cobalt hemoglobin (Hb_{Co}). In order to clarify the complicated multiple interactions, we have diagramatically represented the observed spectra in Figure 3, including separate sets of vertical lines for each component of the spectrum (i.e., sets for the histidine modes and ν(O–O) modes). In the figure, the inherent frequencies of coordinated histidine and dioxygen are depicted with dotted and broken lines, respectively, while the solid lines represent the calculated perturbed frequencies. It should be emphasized that this diagram is not intended to provide an accurate representation of the calculated relative intensities. Those are given in Table I.

The $^{16}O_2$ adduct in H_2O exhibits an intense feature at ~1136 cm^{-1} (overlapped by two strong macrocycle modes) and two secondary features at ~1107 (weak) and 1150 cm^{-1} (medium). In ^2H_2O, the 1150-cm^{-1} feature disappears, and the 1136-cm^{-1} band shifts up to ~1140 cm^{-1}. In the case of the $^{18}O_2$ adduct in ^1H_2O, a strong band is observed at 1063 cm^{-1} along with a medium intensity feature at 1093 cm^{-1}, both of which are not present for the $^{16}O_2$ adduct (i.e., they are associated with the $^{18}O_2$ adduct). In ^2H_2O, the strong 1063-cm^{-1} band shifts *up* to 1070 cm^{-1}, and the 1093-cm^{-1} feature *apparently* is not altered (vide infra). The spectra of the adducts with scrambled O_2 contain contributions from the $^{16}O_2$ and $^{18}O_2$ adducts as well as the $^{16}O^{18}O$ adduct. In ^1H_2O a relatively strong band at 1098 cm^{-1} is observed along with a very weak feature at ~1080 cm^{-1}. The corresponding spectrum in ^2H_2O exhibits the 1098-cm^{-1} band but the weak 1080-cm^{-1} mode disappears.

The observed frequencies and approximate intensities of all of these features are predicted by eq 1 and 3, given the following well-supported assumptions. There is only one O_2 adduct present whose inherent ν(O–O) frequencies are $\nu(^{16}O–^{16}O)$ = 1139 cm^{-1}, $\nu(^{16}O^{18}O)$ = 1106 cm^{-1}, and $\nu(^{18}O–^{18}O)$ = 1073 cm^{-1} [note $\Delta\nu(^{16}O_2/^{16}O^{18}O) = \Delta\nu(^{16}O^{18}O/^{18}O_2)$ = 33 cm^{-1}]. The histidyl-imidazole fragment possesses internal modes at 1148, 1109, and 1085 cm^{-1} in ^1H_2O, but in ^2H_2O exchange of the N^1H to N^2H

(26) We note only slight discrepancies between the data published in ref 9, 11, and 29 (i.e., frequencies are within 2 cm^{-1}). To facilitate comparison of observed and calculated frequencies and intensities we have used data from ref 11. However, we note that the data presented in ref 9 is of generally higher quality, but spectra were not obtained in ^2H_2O solution.

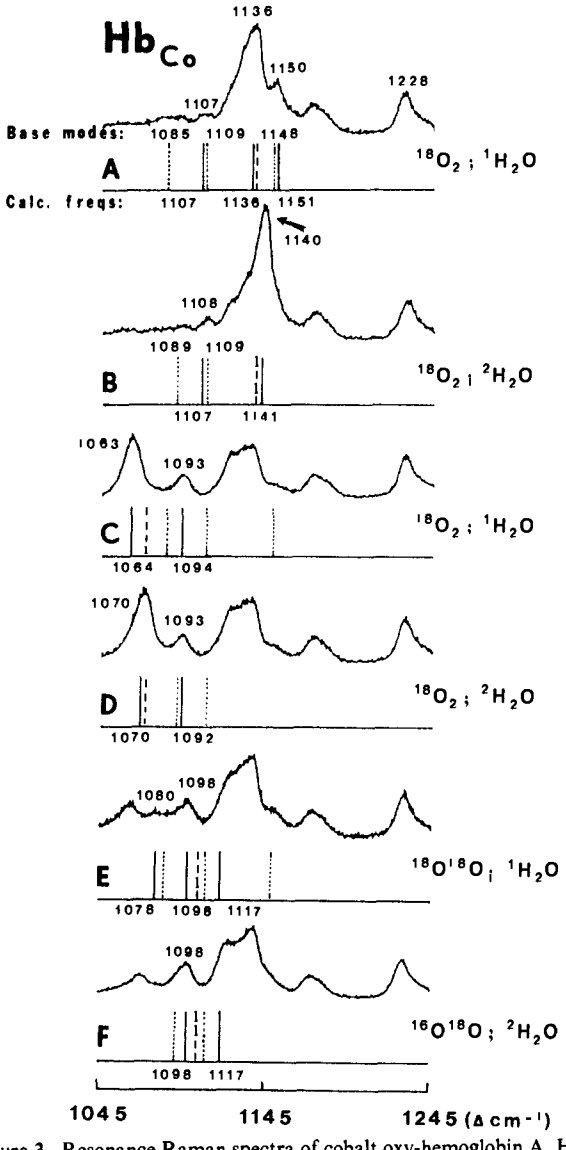

Figure 3. Resonance Raman spectra of cobalt oxy-hemoglobin A, Hb_{Co}, in 50 mM Tris·HCl buffer (H_2O or ^2H_2O), pH (pD) = 8.2, excitation at 406.7 nm. Vertical lines represent the following: dotted (···) inherent frequencies of coordinated histidine; broken (– –) inherent frequencies of coordinated O_2; and solid lines (—), calculated perturbed frequencies of coordinated O_2 and histidine.

alters the internal modes as follows: the 1148- and 1109-cm^{-1} bands are replaced by bands at 1109 and ~1089 cm^{-1}, while the 1085-cm^{-1} band disappears. These assumed histidylimidazole modes are entirely consistent with previously reported data.[27] Thus, free histidine in H_2O (pH = 8.2) exhibits bands at 1158 (br), 1108, 1093, and 1070 cm^{-1}. In ^2H_2O, only two bands are observed in this region: a relatively strong band at 1097 cm^{-1} and a weak band at 1107 cm^{-1}. As has been previously demonstrated,[28] these histidylimidazole modes may shift slightly upon coordination.

The calculated perturbed frequencies and their intensities are given in Table I and illustrated with solid vertical lines in Figure 3. Thus, coupling of $\nu(^{16}O–^{16}O)$ with the nearby (δ = 10 cm^{-1}) 1148-cm^{-1} mode results in a decrease of "$\nu(^{16}O–^{16}O)$" to 1136 cm^{-1} and moderate intensity in the 1151-cm^{-1} "ligand mode". The 1109-cm^{-1} mode is also weakly coupled to $\nu(^{16}O–^{16}O)$ (δ = 30 cm^{-1}) as is evidenced by its weak activation and small shift (2 cm^{-1}) to 1107 cm^{-1}. Upon removal of the interaction with the 1148-cm^{-1} mode (i.e., in ^2H_2O), the $\nu(^{16}O–^{16}O)$ shifts up from 1139 to ~1141 cm^{-1} by virtue of the persistent interaction with the "unchanged" 1109-cm^{-1} ligand mode. This accounts for the observed disappearance of the 1150-cm^{-1} feature and the ~5-cm^{-1} increase of the "$\nu(^{16}O–^{16}O)$".[9,11,29]

The $\nu(^{18}O–^{18}O)$, having an inherent frequency of 1073 cm^{-1}, is strongly coupled with the 1085-cm^{-1} imidazole mode (W_{ni} = 13.75 cm^{-1}, δ = 12 cm^{-1}) to yield perturbed modes at ~1063 and ~1093 cm^{-1} whose calculated intensities approximately match those observed (Table I). In ^2H_2O, the 1085-cm^{-1} imidazole mode is absent, and "$\nu(^{18}O–^{18}O)$" shifts up, approaching its inherent frequency of 1073 cm^{-1}. However, interaction of the internal mode of the *N*-deuteriated histidylimidazole fragment (assumed frequency of 1089 cm^{-1}) with $\nu(^{18}O–^{18}O)$ yields perturbed bands at 1070 and 1092 cm^{-1}. The observed relative intensities also approximately agree with those calculated.

The behavior of the $^{16}O^{18}O$ adduct provides particularly convincing support for this interpretation. The $\nu(^{16}O–^{18}O)$ (inherent frequency = 1106 cm^{-1}) strongly interacts with the 1109-cm^{-1} imidazole mode to yield perturbed bands at ~1098 and 1117 cm^{-1} (the latter is obscured by overlap with the porphyrin mode at ~1120 cm^{-1}). The observed intensity of the "$\nu(^{16}O–^{18}O)$" band relative to that of the "$\nu(^{18}O–^{18}O)$" band at 1063 cm^{-1} also provides strong support on the following grounds. The population ratio of the $^{16}O^{18}O$ and $^{18}O_2$ is 2:1, implying that the intensity of the "$\nu(^{16}O–^{18}O)$" should be twice that of the "$\nu(^{18}O–^{18}O)$". The experimental ratio is only ~1.5. By using the calculated intensities in Table I, it is determined that the 1098-cm^{-1} feature represents only ~56% of the total "$\nu(^{16}O–^{18}O)$" intensity, while the 1063-cm^{-1} feature represents 70% of the total "$\nu(^{18}O–^{18}O)$" intensity. The calculated intensity ratio is thus ~1.5, i.e., in good agreement with that observed. It is especially important to note that the observed behavior for the $^{16}O^{18}O$ adduct is reproduced by using a $W_{ni}(^{16}O^{18}O)$ which is that required on the basis of reduced mass considerations (i.e., $W_{ni}(^{16}O^{18}O)$ = 0.985 $W_{ni}(^{16}O_2)$ or 9.38 = (0.985) × 9.52). The observation of a weak feature near 1080 cm^{-1} for the ($^{16}O–^{18}O$) adduct in ^1H_2O, which disappears in ^2H_2O, is also readily explained. Thus, $\nu(^{16}O–^{18}O)$ interacts with the 1085-cm^{-1} ligand mode to yield a perturbed mode at ~1080 cm^{-1} (1078 cm^{-1} calculated) (Table I). In ^2H_2O, the 1085-cm^{-1} mode is absent, and the corresponding weak ~1080-cm^{-1} (coupled) mode also disappears, as expected.

In summary of this section, the complex spectral patterns observed for the proteins is satisfactorily explained by invoking vibrational coupling of ν(O–O) with internal modes of the proximal histidylimidazole. Using the conventional Fermi resonance coupling scheme, all of the calculated frequencies and intensities are shown to be in reasonable agreement with those observed (although several features are obscured by overlap with porphyrin macrocycle modes and accurate intensity measurements are not possible). To obtain this satisfactory agreement between the observed and calculated spectral patterns it is only necessary to assume the existence of histidylimidazole modes at 1148, 1108, and 1085 cm^{-1} in ^1H_2O and 1108 and 1089 cm^{-1} in ^2H_2O. These assumed frequency values are quite close to those observed in the spectra of free histidine.[27] All of these modes are apparently of *A'* symmetry, thus they can couple with the ν(O–O) mode.[27a,c]

This quantitative treatment of the oxy-Hb_{Co} spectral patterns strengthens the more qualitative arguments presented in our earlier work[11] and supports the interpretation given there. Thus, the observed spectra do not require the existence of two stable structures as had been previously argued.[7,9]

D. Summary and Conclusions. The complex spectral patterns observed in the resonance Raman spectra of O_2 adducts of cobalt-substituted heme proteins and model compounds are shown to result from vibrational coupling of ν(O–O) with internal modes of the trans-coordinated axial ligand. The conventional "Fermi resonance" equations[17] can be employed to demonstrate that all of the experimental data are consistent with theory. Recent theoretical treatments validate the use of these equations for

(27) (a) Ashikawa, I.; Itoh, K. *Biopolymers* **1979**, *18*, 1859. (b) Bruha, A.; Proniewicz, L. M.; Kincaid, J. R. Unpublished results. (c) Hodgson, J. B.; Percy, G. C.; Thornton, D. A. *J. Mol. Struct.* **1980**, 66, 75, and 81.
(28) (a) Salama, S.; Spiro, T. G. *J. Am. Chem. Soc.* **1978**, *100*, 1105. (b) Walters, M. A.; Spiro, T. G. *Inorg. Chem.* **1983**, *22*, 4014.

(29) Kitagawa, T.; Ondrias, M. R.; Rousseau, D. L.; Ikeda-Saito, M.; Yonetani, T. *Nature (London)* **1982**, *298*, 869.

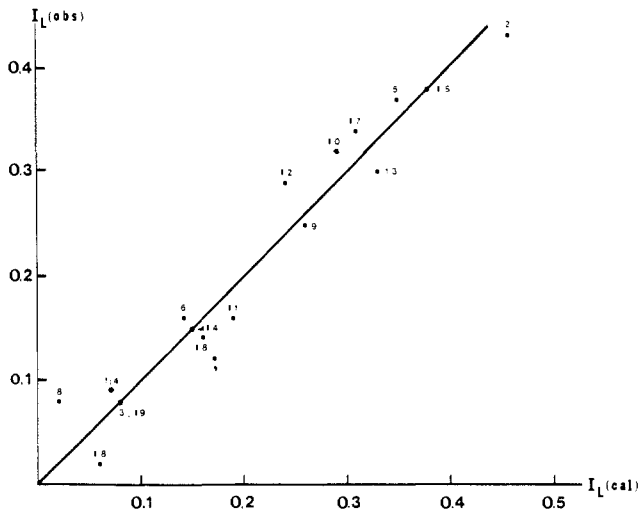

Figure 4. Plot of observed vs calculated ligand intensity I_L.

interactions of two fundamental modes.[24,25] The excellent agreement between theory and experiment is illustrated in Figure 4. The greater scatter at low values of I_L is the result of greater experimental uncertainty in determining the intensities of weak bands.

While the existence of such complications underscore the need for high-quality spectra and cautious interpretation, the present study demonstrates the potential utility of such vibrational interactions. Thus, utilization of multiple isotopomers and careful analysis of resulting spectra can provide accurate estimates for the frequencies of some coordinated histidylimidazole internal modes; information which is otherwise not directly available.[30]

Finally, it is interesting to consider other possible coupling interactions and their potential utility. Thus, we are now making efforts to identify such interactions in dioxygen, carbon monoxide, nitric oxide, and cyanide derivatives of heme proteins and model systems. Such studies are generally focussed on the low frequency region where modes such as ν(Fe–CN), ν(Fe–NO), ν(Fe–CO), ν(Fe–O_2), δ(FeOO), δ(FeCO), δ(FeCN), ν(Co–O_2), and δ(CoOO) may interact with lower frequency histidylimidazole modes. In this way, additional histidylimidazole modes, including ν(Fe–N_{his}), may be observed.

Acknowledgment. We express our sincere thanks to Professor Dennis Strommen of Carthage College for help with the BASIC program and Professor Jeanne McHale for providing a copy of her manuscript prior to publication. L.M.P. acknowledges Grant No. RP-11-13 provided by the Polish Ministry of Education. This work was supported by the National Institutes of Health (Grant No. DK35153 to J.R.K.).

Registry No. O_2, 7782-44-7; Λ-[Co(en)$_2$(*S*-Ala)]$^{2+}$, 28459-63-4; Δ-[Co(en)$_2$(*S*-Ala)]$^{2+}$, 28536-95-0; Λ-[Co(en)$_2$(*S*-Phe)]I_2, 123881-50-5; Δ-[Co(en)$_2$(*S*-Phe)]I_2, 123881-51-6; Λ-[Co(en)$_2$(*S*-Phe)]$(ClO_4)_2$, 123881-52-7; Δ-[Co(en)$_2$(*S*-Phe)]$(ClO_4)_2$, 39000-16-3; Λ-[Co(en)$_2$(*S*-Val)]I_2, 123881-53-8; Δ-[Co(en)$_2$(*S*-Val)]I_2, 123881-54-9; Λ-[Co(en)$_2$(*S*-Val)]Br_2, 123881-55-0; Δ-[Co(en)$_2$(*S*-Val)]Br_2, 123881-56-1; Λ-[Co(en)$_2$(*S*-Glu)]ClO_4, 16040-63-4; Δ-[Co(en)$_2$(*S*-Glu)]ClO_4, 33293-37-7; Λ-[Co(en)$_2$(*S*-Asp)]ClO_4, 33864-49-2; Δ-[Co(en)$_2$(*S*-Asp)]ClO_4, 33864-50-5; Δ,Λ-[Co(en)$_2$(*S*,*R*-AspH)]Cl_2, 123932-07-0; Δ,Λ-[Co(en)$_2$(*R*,*S*-Val)]Cl_2, 123881-57-2; Λ-[Co(en)$_2$(Gly)]$^{2+}$, 19657-80-8; Δ-[Co(en)$_2$(Gly)]$^{2+}$, 19657-79-5; H_2, 1333-74-0.

(30) Caswell, D. S.; Spiro, T. G. *J. Am. Chem. Soc.* **1986**, *108*, 6470.

Phosphate Ester and Phosphinate Binding to the (μ-Oxo)diiron(III) Core: Synthesis and Characterization of $[Fe_2O\{O_2P(OC_6H_5)_2\}_2(HBpz_3)_2]$ and $[Fe_2O\{O_2P(C_6H_5)_2\}_2(HBpz_3)_2]$

Petra N. Turowski, William H. Armstrong, Mary E. Roth, and Stephen J. Lippard*

Contribution from the Department of Chemistry, Massachusetts Institute of Technology, Cambridge, Massachusetts 02139. *Received June 7, 1989*

Abstract: To model the interaction of phosphate ligands with oxo-bridged diiron proteins, (μ-oxo)bis(μ-diphenyl phosphato)bis(hydrotris(1-pyrazolyl)borato)diiron(III) (**1**) and (μ-oxo)bis(μ-diphenylphosphinato)bis(hydrotris(1-pyrazolyl)borato)diiron(III) (**2**) were prepared. X-ray crystallographic studies reveal that the diiron(III) core is expanded in both compounds relative to dicarboxylate-bridged proteins and model compounds. Fe–O–Fe bond angles of 134.7 (2) and 130.6 (3)°, and Fe···Fe distances of 3.335 (1) and 3.292 (2) Å were observed for **1** and **2**, respectively, and the symmetric Fe–O–Fe stretching vibrations at 478 and 485 cm^{-1} have lower energies than those of other triply-bridged diiron(III) compounds. The Fe–O_{oxo} bond distances in **1** and **2**, 1.808 (3) and 1.812 (3) Å, are longer than observed in analogous dicarboxylate bridged compounds, and, consequently, the antiferromagnetic spin exchange coupling constants, −97.5 (1) and −93 (1) cm^{-1}, are smaller in magnitude than usually found in such oxo-bridged diiron(III) compounds. Interactions with the paramagnetic metal centers shift the ^1H NMR signals by up to 6.5 ppm downfield from free ligand values. NMR assignments were facilitated by determination of T_1 relaxation times. As for purple acid phosphatases, no signals were observed in the ^{31}P NMR spectra of either model compound. Mössbauer and electronic spectral parameters resemble those of dicarboxylate-bridged (μ-oxo)diiron(III) model compounds. The phosphate ester and phosphinate bridged model complexes do not exhibit the unusual spectroscopic features of purple acid phosphatases, suggesting that these proteins are unlikely to have a (μ-oxo)(μ-phosphato)diiron(III) center.

Interactions of phosphate[1] ligands with oxo-bridged diiron units are potentially important in proteins such as purple acid phosphatases from bovine spleen[2] and porcine allantoic fluid,[3] ribonucleotide reductase from *E. coli*,[4] the invertebrate respiratory

0002-7863/90/1512-681$02.50/0